





How do stream processes affect hazard exposure on alluvial fans? Insights from an experimental study

Bruno MAZZORANA^{1,2,3*}  <https://orcid.org/0000-0003-1218-4495>;  e-mail: bruno.mazzorana@uach.cl

Elisa GHIANDONI⁴  <https://orcid.org/0000-0002-8277-9278>; e-mail: ghiandonielisa@gmail.com

Lorenzo PICCO^{2,3,4}  <https://orcid.org/0000-0001-5265-2797>; e-mail: Lorenzo.picco@unipd.it

*Corresponding author

¹ Universidad Austral de Chile, Faculty of Sciences, Instituto de Ciencias de la Tierra, 5090000 Valdivia, Chile

² Universidad Austral de Chile, RINA – Natural and Anthropogenic Risks Research Center, 5090000 Valdivia, Chile

³ Universidad Austral de Chile, Laboratory of Hydromorphology, Faculty of Forest Sciences and Natural Resources, 5090000 Valdivia, Chile

⁴ University of Padova, Department of Land, Environment, Agriculture and Forestry, 35020 Legnaro, Italy

Citation: Mazzorana B, Ghiandoni E, Picco L (2020) How do stream processes affect hazard exposure on alluvial fans? Insights from an experimental study. *Journal of Mountain Science* 17(4). <https://doi.org/10.1007/s11629-019-5788-x>

© Science Press, Institute of Mountain Hazards and Environment, CAS and Springer-Verlag GmbH Germany, part of Springer Nature 2020

Abstract: Alluvial fans are among the most privileged settlement areas in many mountain regions. These landforms are particularly dynamic being episodically affected by distributary processes generated by extreme flood events. Addressing risk assessment entails determining hazard exposure and unravelling how it might be related to process loading and to process dynamics once the flow becomes unconfined on the surface of alluvial fans. By following a ‘similarity of process concept’, rather than by attempting to scale a real-world prototype, we performed a set of 72 experimental runs on an alluvial fan model. Thereby, we considered two model layouts, one without a guiding channel and featuring a convex shape and the other one with a guiding channel, a bridge, and inclined but planar overland flow areas as to mirror an anthropic environment. Process magnitude and intensity parameters were systematically varied, and the associated biphasic distributary processes video recorded. For each experiment, the exposure was detected by mapping the exposed area in a GIS, thereby discerning between

areas exposed to biphasic flows and the associated depositional phenomena or to the liquid flow phase only. Our results reveal that total event volume, sediment availability and stream power in the feeding channel, as well as depositional effects, avulsion, and channelization on the alluvial fan concur to determine the overall exposure. Stream process loading alone, even when rigorously defined in terms of its characterizing parameters, is not sufficient to exhaustively determine exposure. Hence, further developing reliable biphasic simulation models for hazard assessment on settled alluvial fans is pivotal.

Keywords: Alluvial fan; Hazard; Exposure; Flood risk; Experimental model; Process similarity

Introduction

Alluvial fans are depositional landforms common in almost all climatic environments of the world (Antronico et al. 2015) exerting a direct control on sediment transfer in mountainous watersheds as temporary storage areas. Typically,

Received: 15-Sep-2019

1st Revision: 23-Dec-2019

2nd Revision: 27-Feb-2020

Accepted: 04-Mar-2020

these depositional forms evolve in piedmont areas, usually at the exit of narrow and steep valleys, due to the difference between the upstream and the downstream sediment transport capacity (Bull 1977). Because they affect the sediment dynamics downstream retaining sediments, they play an important role in the entire riverine geomorphology (Clarke 2015). They spread in a radiating pattern forming conical bodies having concave long profile and convex cross profile, starting from a single topographic apex (Drew 1873; Clevis et al. 2003). Their angle of expansion typically varies between 15°-90° (Blair and McPherson 2009). Alluvial fans usually extend for 0.5-10.0 km onto the plain (Anstey 1965) and with increasing distance from their apexes, their surface can be conveniently subdivided into a proximal, a medial, and a distal part (Sanchez-Nuñez et al. 2015).

Alluvial fans are usually classified into two main categories, debris-flow fans and fluvial-based fans, according to the behavior of predominant processes reaching the fan apex, which are triggered in the contributing hydrological basin and propagate along its stream network (Blair and McPherson 1994). Worldwide, local communities seem to largely ignore the risk related to distributary processes on alluvial fans, which is expressed by an equation that includes the probability of occurrence of the underlying hazard scenario (Mazzorana et al. 2012), the exposure (Fuchs et al. 2015), the vulnerability of the elements at risk (Papathoma-Köhle et al. 2017), and their related value (Fuchs 2009; Mazzorana and Fuchs 2010; Mazzorana et al. 2012). In fact, especially in alpine valleys people continue to move into these flood prone areas for residential and socio-economic purposes due to the morphological constraints of the harsh environment and because these landforms have been since long time the preferred areas for agricultural activities (Pelletier et al. 2005; Santangelo et al. 2011; Kain et al. 2018). When considering the ongoing climate change and the associated increased frequency of weather extremes (De Haas et al. 2018), a more intense response in terms of debris flows and sediment laden flows can be expected (Antronico et al. 2015). Due to the increased exposure, negative repercussions in terms of expected losses might be considerably severe for the affected communities

(Mazzorana and Fuchs 2010; Fuchs et al. 2017a, b). As the direct utility of preventively reducing hazard exposure is undisputedly reckoned (Röthlisberger et al. 2017), societies should attempt to implement an optimal bundle of preventive strategies, mitigation measures as well as increase their preparedness and response capacities ultimately resulting into an effective hazard adaptation (Mazzorana et al. 2017a; Mazzorana et al. 2018).

Our study specifically aims at refining the understanding of how exposure is influenced by the hazard process characteristics on alluvial fans, thereby neglecting any co-determining role of economic growth and societal pressure. In particular, the relation between a set of process characteristics and the resulting exposure is experimentally investigated.

Experimental alluvial fan models are useful research tools to study alluvial processes and have been largely adopted also by hydro-geomorphologists (Hooke 1968; D'Agostino et al. 2009; Clarke 2015). In fact, field techniques alone do not allow for continuous real time observations over sufficiently large time spans which are consistent with the geomorphological time scale at which fan evolution occurs (Clarke et al. 2010; Harvey 2012). Moreover, the high number of variables interacting in alluvial fan systems makes the understanding of their dynamics quite complex, as the isolation of individual variables might be difficult when dealing with catchment, climate, tectonic, and internal system features (Clarke 2015). By following the 'similarity of process concept' (Hooke 1968), important advances could be achieved in determining the primary factors influencing alluvial fan dynamics, such as slope (Hooke 1968; Guerit et al. 2014), avulsion (Bryant et al. 1995; Reitz and Jerolmack 2012), autogenic processes (Muto et al. 2007; Van Dijk et al. 2012), and risk (Davies et al. 2003). However, this approach has also some limitations. In particular, scaling problems need to be addressed, as they can often distort certain flow processes and the resulting morphologies, thus a special attention must be devoted when transferring experimental findings to a field setting (Paola 2009; Sturm et al. 2018a,b). Through an extended literature review (Magilligan 1992; Cenderelli and Wohl 2003; Dean and Schmidt 2013; Salgueiro et al. 2013; Rainato et al. 2017; Gray et al. 2018) we found that the

concept of event magnitude lacks an unambiguous definition and is quantified through a multitude of proxies and not always univocally determined parameters. Due to this shortcoming, in this study we will a) describe the set of employed system loading variables, which, if properly specified, enables a comprehensive assessment of the conditions the studied system is subjected to; b) explore which loading conditions and specific alluvial fan layouts, viewed in conjunction, exert a tangible influence on exposure as a result of the morphodynamic processes at work; c) examine whether more extreme values of loading variables consistently result into higher exposure on the fan surface.

1 Materials and Methods

Field work methods and computational approaches used in synergy are indispensable and complementary in attempting to accurately mirror morphodynamic processes on alluvial fans, but they are still partially capable to provide the complete picture and to identify and quantify all intervening key factors and components. Hence, applying the experimental approach is, despite the limitations and drawbacks outlined earlier, a promising way to integrate the traditional approaches and to generate knowledge with respect to the aforementioned theoretical research questions that motivated this study (Clarke 2015). Based on this rationale, the research strategy of this study is founded on three pillars:

i) The quantification of exposure and the qualitative assessment of the underlying distributary dynamics and related phenomena, with respect to the analysis of the generated system response, coherently with the defined research questions and the adopted ‘similarity of process concept’ concept (Clarke 2015);

ii) The use of a basic experimental setup, which, despite its simplicity, features the required parameters, allowing the definition and measurement of the system loading parameters (Sturm et al. 2018b);

iii) The modular system layout, for agile prototyping and rapid execution of the single experimental runs (Mazzorana et al. 2017b).

It must be underlined that the experimental

setup used in this study did not allow reproducing the whole array of situations occurring in nature, because the adopted alluvial fan surface is non-erodible, therefore channel incision is only possible on the previously deposited lobes and its vertical extent is limited by the non-erodible fan surface elevation. In addition, observed process dynamics are only macroscopically similar within the context of the similitude-by-process approach, which means that physical processes occurring in nature may only partially be reproduced. Anyway, despite the presence of the non-erodible surface, understanding the peculiarities of distributary processes, where channel incision below the original fan surface is not to be expected, is not precluded. Moreover, this setting is useful for capturing channelization and self-confining flows on previously deposited material.

The experimental model presents three movable components: the alluvial fan, the tank, and the feeding channel, which links the two.

The dimensions of the model are reported in Figure 1. Two alluvial fan settings were employed: a) the “unchanneled” alluvial fan (hereinafter *UC*), which mirrors a typical convex-shaped, non-modified alluvial fan, and b) the “artificially channeled” alluvial fan (hereinafter *AC*), which simulates an alluvial fan modified by human intervention and characterized by the presence of a guiding channel along its symmetry axis, a bridge crossing the channel, and plain lateral alluvial areas (Figure 1).

The surface of *UC* is 21.41 dm² and is composed by PEVA, which provides some roughness to the model as to simulate real fan conditions, whereas *AC* is 15.26 dm² and is built with expanse PVC, having a lower roughness than *UC*. The feeding channel spills on the fan surfaces, but in *AC* water is guided in the channelized path in the middle of the fan, constraining and giving a predefined direction to the flow that, in the lower part of the fan, passes below the bridge. The area where the alluvial fan is placed is surrounded by a containment rubber pool to prevent water and sediment to leave the system. The tap regulating the flow of water from the tank is set 42.0 cm above the base of the system and it is opened in order to determine a medium or a full stream power. The channel is 5.7 cm × 54 cm × 20 cm (Figure 1). In the upper segment, the water gets in

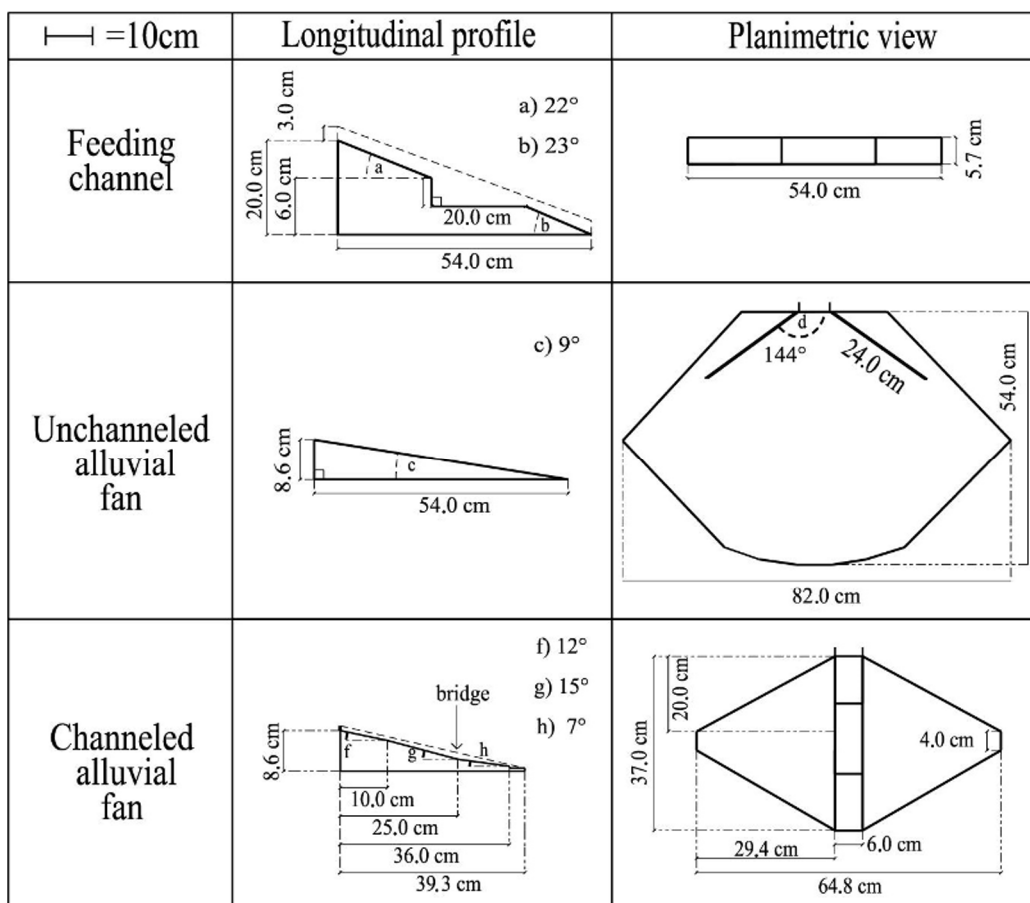


Figure 1 Longitudinal profile (middle column) and planimetric view (right column) of the model components: feeding channel, the unchanneled (UC) alluvial fan and the artificially channeled (AC) alluvial fan model (displayed top-down in this sequence).

touch with the channel at a height of 26.0 cm from the base. The middle segment has a vertical step followed by a tract with null slope; this simulates the area where the stored sediment can be entrained by water and the biphasic flow is initiated. The downstream segment is connected to the alluvial fan. The specifications of the recording camera are: 13 Megapixel, Full HD, 30 fps, auto focus enabled. The sediment material is quartz, with a known density of 2.58 g/cm³, and its grain size varies between 1 and 2 mm.

1.1 Experimental design

To explore how a specific loading configuration affects exposure, the decision was to adopt an experimental approach based on the ‘similarity of process concept’ suggested by Hooke in 1968, who stated that natural systems could be reproduced in laboratory settings that are “treated

as small systems in their own right, not as scale models of prototypes”. In the case of this specific study, previously outlined limitations can mostly be neglected, since the aim is investigating the relation between specific loading configurations and the resulting exposure, and not explaining, through a scaled model, the complex physics of the process dynamics occurring on a real alluvial fan.

The common thought suggests that more severe loading configurations necessarily result into higher exposures (i.e. larger exposed areas) on the alluvial fan. However, this statement is particularly problematic for the following interrelated reasons:

1) the most severe loading conditions can be assessed only after the effects in terms of exposure became apparent and, in this respect, the suspicion is that maximum exposure is not necessarily associated with maximum process intensities or magnitudes;

2) maximum geomorphic work does not necessarily result into maximum exposure since the associated morphodynamic effects might, at least partially, become manifest in the third dimension through potentially destructive aggradation and incision processes;

3) biphasic distributary processes are inherently complex and characterized by sudden channel avulsions and re-channelization which may alter exposure to a significant extent.

A total number of 72 experimental runs has been carried out. Each of them tests different values of the loading variables, namely total event volume, stream power regime and sediment volume ratio (sediment volume in the storage wedge of the feeding channel vs. total event volume where the volume of the sediment grains is straightforwardly determined based on their mass and density) (Table 1). The first variable represents the total volume, V_t , (0.7 L, 1.0 L and 1.3 L, respectively) resulting from different combinations of water and sediment (i.e. milky quartz variety for its white color), the second variable accounts for two distinct stream power regimes, Ω , medium stream power (hereinafter Ω_M , corresponding to a half open tap controlling the release of water from the tank), and full stream power (hereinafter Ω_F , corresponding to a fully open tap releasing water from the tank), the third variable, $V_s\%$, indicates the ratio between the available sediment volume in the storage area before each run and the total volume expressed as percentage of the total volume. We refer to these percentages as ‘volumetric sediment percentages’. Volumetric sediment percentages increase from 5% to 30% at steps of 5%.

We remark that two experimental runs with the same initial and boundary conditions may generate fluxes reaching the alluvial fan apex that may exhibit random fluctuations throughout the event duration (Sturm et al. 2018a, b). To facilitate the reader all employed abbreviations are reported in the supplementary material (see Appendix 1).

1.2 Sediment budgeting

In Figure 2 the workflow diagram for the determination of the sediment budgets is shown. After the runs, the sediment was collected according to three storage areas: the not entrained

sediment in feeding channel or not removed from the storage area (Channel - C), the finally deposited sediment on the alluvial fan surface (Fan - F) and in the containment pool (Pool - P). This last compartment, which is not considered part of the active system, was meant to represent a receiving river or a different catchment area, able to collect the sediment leaving the alluvial fan. The collected material was oven-dried at 300°C for 25 minutes and then weighted. If the weighting error exceeded 3% (i.e. final weight compared with the initially

Table 1 Scheme of the experimental design. Total event volumes were chosen according to the dimension of the tank and represent a combination of water and quartz (Alluvial fan types: unchanneled fan (UC) and artificially channeled fan (AC))

Sediment diameter	Alluvial fan type	Stream power	Total event volume V_t (L)	Sediment fraction V_s (%)
1 mm < diameter < 2 mm	UC	Medium	0.7	5,10,15,20,25,30
			1.0	5,10,15,20,25,30
			1.3	5,10,15,20,25,30
		Full	0.7	5,10,15,20,25,30
			1.0	5,10,15,20,25,30
			1.3	5,10,15,20,25,30
	AC	Medium	0.7	5,10,15,20,25,30
			1.0	5,10,15,20,25,30
			1.3	5,10,15,20,25,30
		Full	0.7	5,10,15,20,25,30
			1.0	5,10,15,20,25,30
			1.3	5,10,15,20,25,30

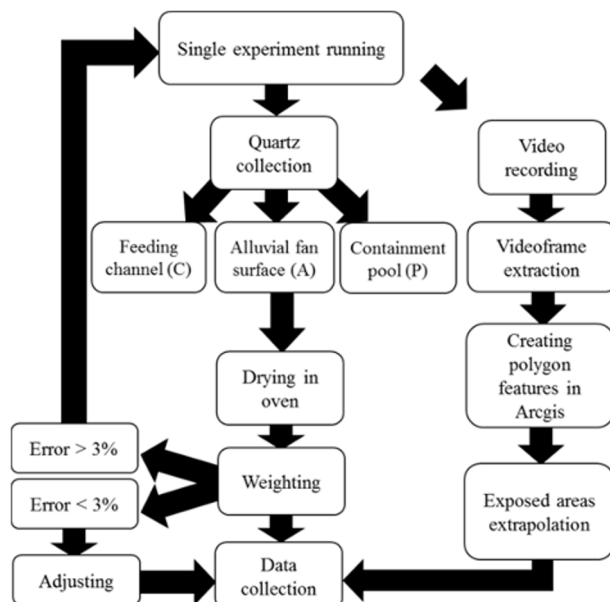


Figure 2 Work flow diagram. Each run is followed by the collection of the deposits according to three areas: the feeding channel (C), the alluvial fan surface (A) and the containment pool (P).

supplied weight of the sediment grains), the whole experiment was repeated. If errors below the threshold of 3% were detected, the missing/exceeding volume would be attributed to the deposition zone with the highest value (Figure 2). For each experimental run we obtained an accurate sediment budget discerning between the weights (i) of the sediment which remained in the channel (w_c or $w_c\%$ if accounted as percentage), (ii) of the deposited sediment on the fan (w_f or $w_f\%$), and (iii) of the exported sediment to pool (w_p or $w_p\%$).

Based on the obtained sediment budgets we analyzed whether, with respect to the two employed alluvial fan layouts (UC and AC , respectively), there were statistically significant differences between the weight (i) of the remaining sediment in the feeding channel (i.e. w_c), (ii) of the deposited sediment on the alluvial fan (i.e. w_f), and (iii) of the exported sediment to the pool (i.e. w_p). Then for alluvial fan layout separately we investigated whether there were statistically significant differences between the weight of the remaining, deposited or exported sediment depending on the applied stream power regime, Ω_M and Ω_F respectively. The analytic procedure entailed, for each weight dataset, examining inferentially by an appropriate hypothesis test (i.e. Shapiro-Wilk test) if the weight data sets were normally distributed. In case of normally distributed datasets we used the Welch's t-test for means comparison, otherwise we employed the Wilcoxon rank sum test for the same purpose.

1.3 Hazard-Exposure Analysis

All the 72 experiments were video recorded. To detect exposure, the recorded videos were processed with a Python script to extract the single video frames showing the total exposure of each experiment. Once identified, these frames were used as base images for ArcGis to draw polygons at real scale and obtain the exposed areas in dm^2 (Figure 3).

Two types of exposure area were considered: the sediment deposition area (DA) and the total exposure area (E) by distinguishing whether we account them in absolute terms or as percentage of the fan area (DA , $DA\%$ and E , $E\%$, respectively). We introduced two subscripts S and W to indicate the components of the biphasic flow, sediment and

water. Hence, DA_s or $DA_s\%$ show where the quartz is deposited in the fan and E_{s+w} or $E_{s+w}\%$ show the maximum flooded area, comprising the zones covered by sediment and water.

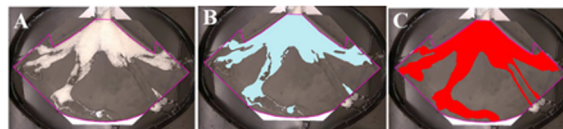


Figure 3 Example of ArcGis polygonation. A) Base image correspondent to the video frame with the maximum exposure detected during the single experiment (total exposure); B) Detection of the sediment deposition areas (light blue); C) Detection of the total exposure (red).

By correlation analysis we explored the relations $w_f \sim DA_s\%$, $w_f \sim E_{w+s}\%$ and $DA_s\% \sim E_{w+s}\%$ for the adopted alluvial fan layout (UC and AC), irrespectively of the adopted stream power regimes and considering them separately.

To assess how hazard (V_t , $V_s\%$) end exposure variables ($DA_s\%$ and $E_{w+s}\%$, respectively) might be correlated among each other we calculated the correlation matrices for the following six settings: UC , AC , $UC + \Omega_M$, $UC + \Omega_F$, $AC + \Omega_M$, $AC + \Omega_F$.

We then complemented hazard-exposure analysis by determining the multiple linear regression models, $DA_s\% = a_0 + a_1V_t + a_2V_s\% + \varepsilon$ and $E_{w+s}\% = a_0 + a_1V_t + a_2V_s\% + \varepsilon$ for the same six settings as an attempt to model the relationships between the response variables, $DA_s\%$ and $E_{w+s}\%$, and hazard (i.e. explanatory variables with assigned values for each experimental setting). This entailed quantifying for each model, the intercept, a_0 , and the angular coefficients, a_1 and a_2 , of the multiple linear regression plane. In these models ε represents the stochastic component.

2 Results

2.1 Sediment budgeting

2.1.1 Descriptive insights

In Figures 4 and 5 the results in terms of sediment budget for all exponential runs are shown. When considering the UC fan results (Figure 4), it is possible to visually appreciate, for both Ω_M and Ω_F , increasing weight values of deposited sediment on the fan surface if the total event volume is

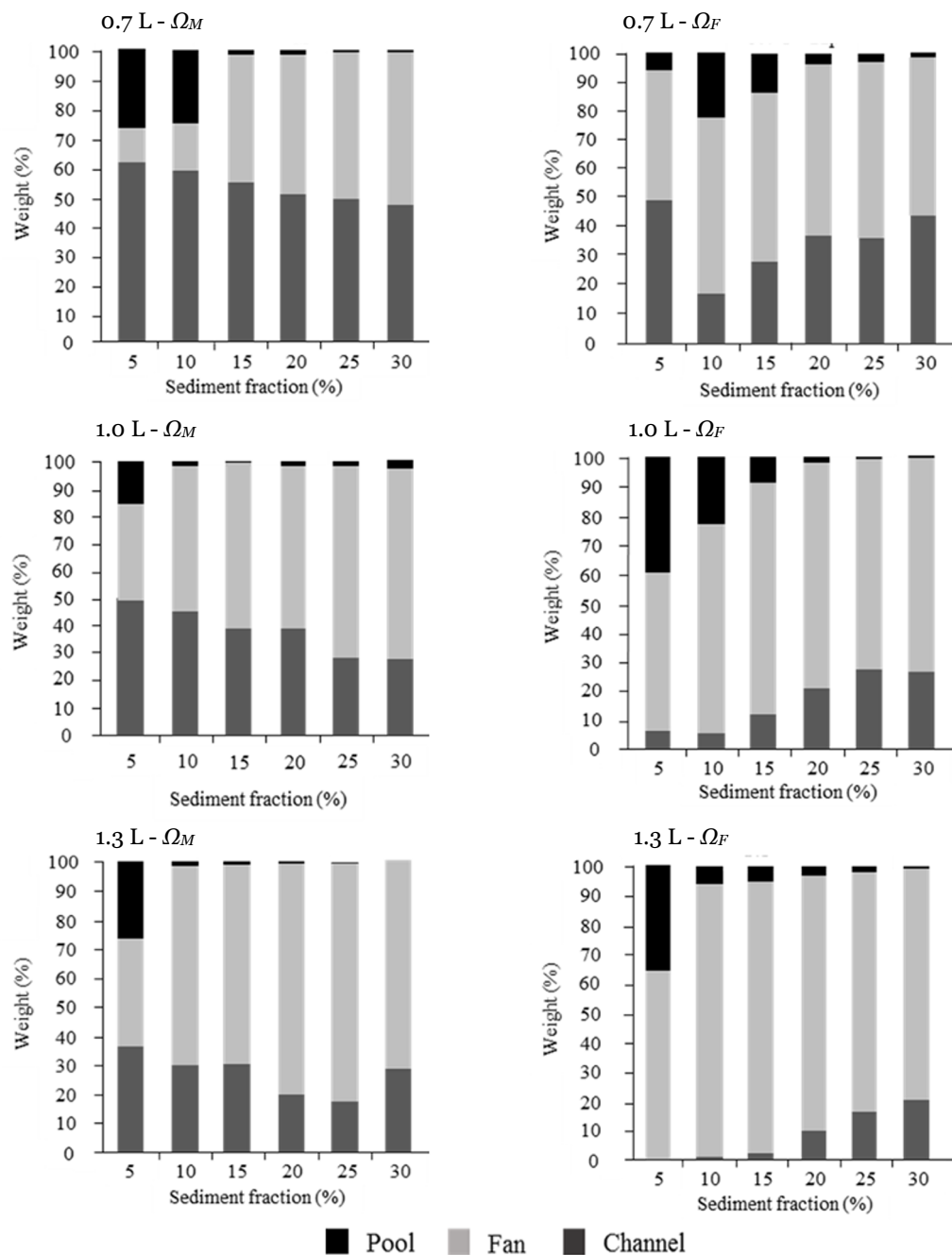


Figure 4 Sediment budget results for the unchanneled alluvial fan (*UC*), experiments run by applying a Ω_M regime and a Ω_F regime shown on the left and right side, respectively and by employing a total volume of 0.7 L (two graphs in the upper part), 1.0 L (two graphs in the middle part) and 1.3 L (two graphs in the lower part). Abbreviations used: Ω_M =medium stream power; Ω_F = full stream power; *C* = channel; *F* = alluvial fan surface; *P* = pool.

increased from 0.7 to 1.3 L, and, in parallel, a reduction of the residual sediment volume stored in the feeding channel can be detected.

Ω_F determined that higher volumes of sediment were transported to the fan and ultimately delivered to the pool. Increasing the volumetric sediment percentage, the deposition on the fan increased when releasing water at Ω_M , while

at Ω_F this pattern could be observed only for volumetric sediment percentages lower or equal to 15%, whereas for larger volumetric sediment percentages slight decrease were detected.

As far as *AC* is concerned (Figure 5), similar results were obtained, except when considering a total volume of 1.3 l and releasing water with Ω_M . In this case, the highest volumetric sediment

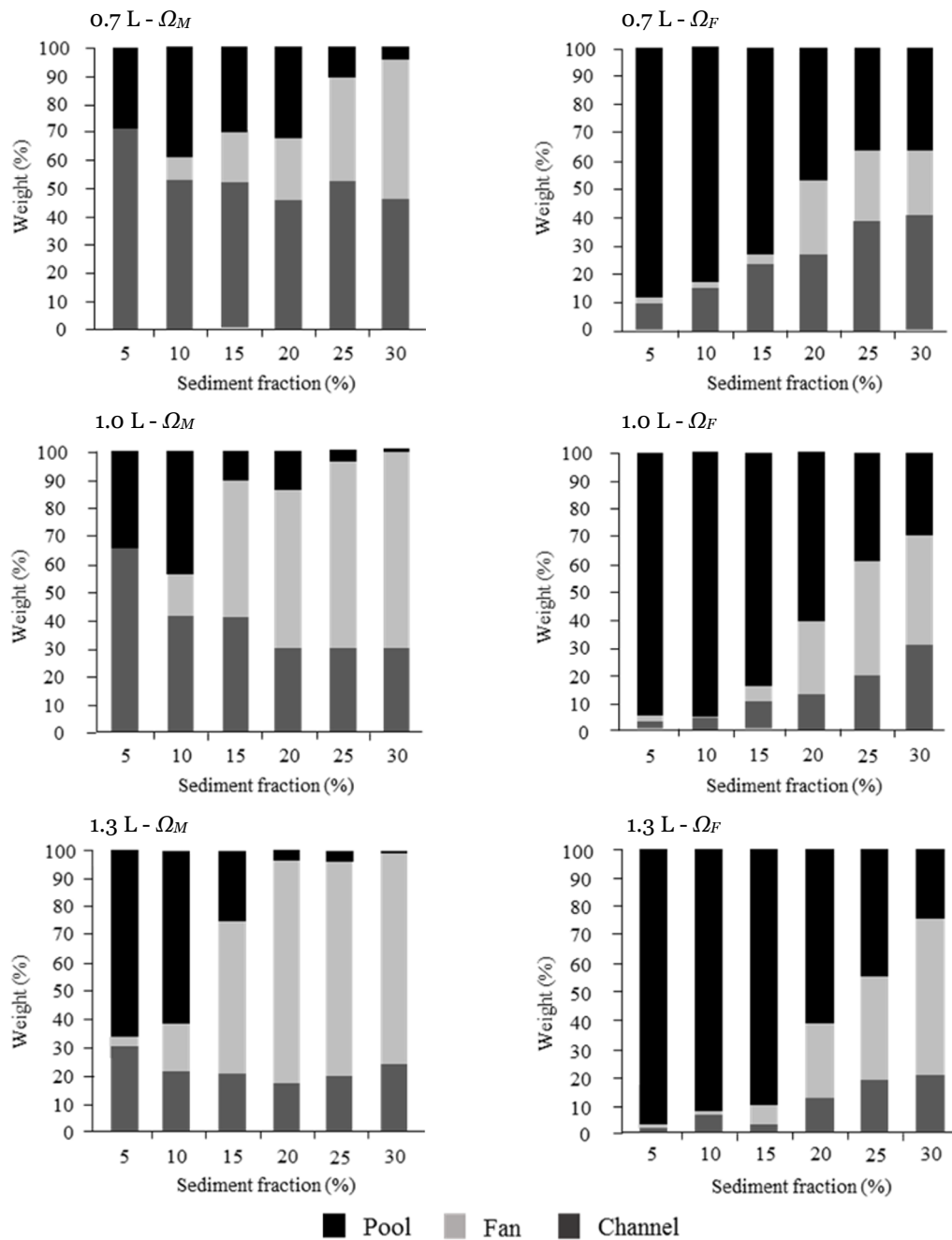


Figure 5 Sediment budget results for the artificially channeled alluvial fan (AC); experiments run by applying the Ω_M regime and the Ω_F regime shown on the left and right side, respectively and by employing a total volume of 0.7 L (two graphs in the upper part), 1.0 L (two graphs in the middle part) and 1.3 L (two graphs in the lower part). Abbreviations used: Ω_M =medium stream power; Ω_F = full stream power; C = channel; F = alluvial fan surface; P = pool.

percentage (30%) did not correspond to the maximum volume of sediment deposited on the fan. Moreover, applying Ω_F , a minor sediment deposition on the fan could be spotted when compared with the experimental runs conducted with Ω_M . In the discussion section we identify and

visualize the suit of geomorphic processes at work directly influencing the distributary dynamics and potentially altering the sediment budgets as previously observed.

The major difference emerging between the UC alluvial fan and the AC alluvial fan resides in

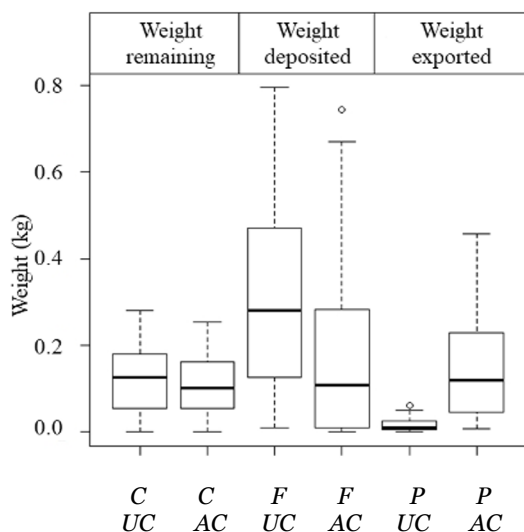


Figure 6 Boxplots of the weights (kg) remaining in the feeding channel (C), deposited on the alluvial fan (F) and exported to the pool (P) for both alluvial fan layouts (unchanneled (UC) and artificially channeled (AC), respectively) but not distinguishing between the applied stream power regimes.

the amount of sediment reaching the pool, which was consistently higher in the latter case (AC) for both stream power regimes. Plausible reasons for these results might be related to the presence of the guiding channel that could have increased the transfer capacity for the transported sediment and the lower roughness of the surface of the AC alluvial fan.

2.1.2 Statistical Inference

In Figures 6 and 7 the sediment budgets are summarized in form of boxplot charts. Whereas in Figure 6 the boxplots of the weights (kg) remaining in the feeding channel, deposited on the alluvial fan and exported to the pool are shown for both alluvial fan layouts, in Figure 7 we additionally visualize the boxplots of the weights (kg) also depending on the applied stream power regime.

In Table 2 we report the inference on the true difference in means of the compared datasets (i.e., remaining sediment weights in the feeding channel, deposited sediment weights on the alluvial fan, and exported sediment weight to the pool) in the two employed alluvial fan layouts. In Table 3 and 4 we separately considered the same comparisons in the medium and full stream power case.

To select the proper statistical test for comparing the normality of all datasets, the Shapiro-Wilk normality test was applied. If both compared datasets were normally distributed the Welch's t-test was used, otherwise the Wilcoxon rank sum test was applied.

The weights of the sediment remaining in the feeding channel were not significantly different in the experiments conducted with different model layouts. This result was expected since the flow dynamics in the feeding channel was altered in both layouts, by the abrupt change from a confined

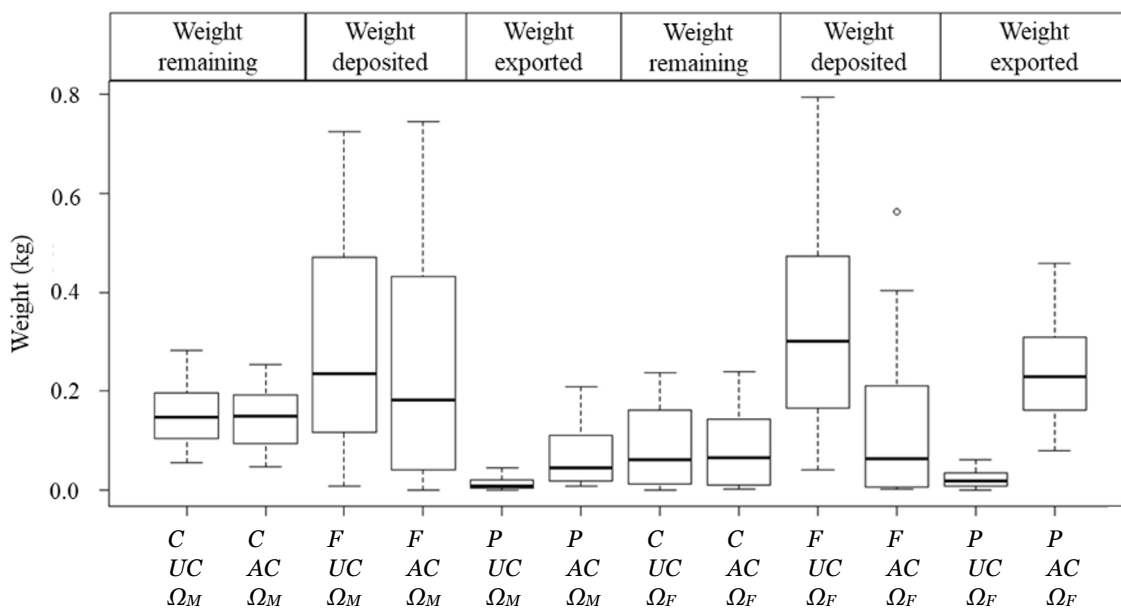


Figure 7 Boxplots of the weights (kg) remaining in the feeding channel (C), deposited on the alluvial fan (F) and exported to the pool (P) for both alluvial fan layouts (unchanneled (UC) and artificially channeled (AC), respectively) and for both applied stream power regimes (Ω_M and Ω_F , respectively).

Table 2 Results of the normality checks for all the weight datasets graphically summarized in Figure 4 by applying the Shapiro-Wilk test and global comparison of the experimental results obtained for the two model layouts (unchanneled (*UC*) and artificially channeled (*AC*), respectively) by comparing the mean weights (kg) of the sediment remaining in the feeding channel, deposited on the alluvial fan and exported to the pool. *C*: feeding channel; *F*: alluvial fan surface; *P*: containment pool.

Part of the system (<i>C, F, P</i>)	<i>C</i>	<i>C</i>	<i>F</i>	<i>F</i>	<i>P</i>	<i>P</i>
Alluvial fan layout (<i>UC, AC</i>)	<i>UC</i>	<i>AC</i>	<i>UC</i>	<i>AC</i>	<i>UC</i>	<i>AC</i>
Weight measures (<i>r</i> = remaining in the feeding channel; <i>d</i> = deposited on the alluvial fan; <i>e</i> = exported to the pool)	<i>r</i>	<i>r</i>	<i>d</i>	<i>d</i>	<i>e</i>	<i>e</i>
Shapiro-Wilk normality test W-value	0.96491	0.94086	0.93965	0.83425	0.84467	0.92098
Shapiro-Wilk normality test p-value	0.3032	0.05402	0.04953	8.43e-05	0.000144	0.01345
Inference on normality on a 0.05 confidence level: (H_0 : data is normally distributed; H_1 : data is no normally distributed)	H_0 accepted	H_0 accepted	H_0 rejected	H_0 rejected	H_0 rejected	H_0 rejected
Welch Two Sample t-test	Yes		No		No	
Wilcoxon rank sum test	No		Yes		Yes	
Test parameter value (and degrees of freedom)	$t = 0.37567$ $df = 69.989$		$W = 897.5$		$W = 125.5$	
p-value	0.7083		0.005041		4.108e-09	
Inference on true difference in means on a 0.05 confidence level: (H_0 : true difference in means is equal to 0; H_1 : true difference in means is not equal to 0)	H_0 accepted		H_0 rejected → the two populations are not identical		H_0 rejected → the two populations are not identical	

Table 3 Results of the normality checks for the weight datasets related to the experiments conducted with medium stream power, Ω_M , graphically summarized in the first 6 boxplots (from left to right) in Figure 5 by applying the Shapiro-Wilk test and specific comparison of the experimental results obtained for the two model layouts (unchanneled (*UC*) and artificially channeled (*AC*), respectively) by comparing the mean weights (kg) of the sediment remaining in the feeding channel, deposited on the alluvial fan and exported to the pool. *C*: feeding channel; *F*: alluvial fan surface; *P*: containment pool.

Part of the system (<i>C, F, P</i>)	<i>C</i>	<i>C</i>	<i>F</i>	<i>F</i>	<i>P</i>	<i>P</i>
Alluvial fan layout (<i>UC, AC</i>)	<i>UC</i>	<i>AC</i>	<i>UC</i>	<i>AC</i>	<i>UC</i>	<i>AC</i>
Stream power regime	Ω_M	Ω_M	Ω_M	Ω_M	Ω_M	Ω_M
Weight measures (<i>r</i> = remaining in the feeding channel; <i>d</i> = deposited on the alluvial fan; <i>e</i> = exported to the pool)	<i>r</i>	<i>r</i>	<i>d</i>	<i>d</i>	<i>e</i>	<i>e</i>
Shapiro-Wilk normality test W-value	0.96941	0.92825	0.92651	0.87058	0.78355	0.87548
Shapiro-Wilk normality test p-value	0.7865	0.1809	0.1686	0.01819	0.000898	0.02193
Inference on normality on a 0.05 confidence level: (H_0 : data is normally distributed; H_1 : data is no normally distributed)	H_0 accepted	H_0 accepted	H_0 accepted	H_0 rejected	H_0 rejected	H_0 rejected
Welch Two Sample t-test applied	Yes		No		No	
Wilcoxon rank sum test	No		Yes		Yes	
Test parameter value (and degrees of freedom)	$t = 0.27023$ $df = 33.918$		$W = 188.5$		$W = 44$	
p-value	0.7886		0.4107		0.0001998	
Inference on true difference in means on a 0.05 confidence level: (H_0 : true difference in means is equal to 0; H_1 : true difference in means is not equal to 0)	H_0 accepted		H_0 accepted		H_0 rejected → the two populations are not identical	

to an unconfined flow setting in *UC* and by back-stepping processes reaching the feeding channel in *AC*. When comparing the deposited weights on the alluvial fan surfaces, the different topographies (and surface roughness) influenced the distributary dynamics remarkably. Indeed, the H_0 hypothesis stating that the true difference in means is equal to 0 could not be accepted. As foreseeable, we

detected also statistically significant differences between the two model layouts in relation to the weights of the sediment exported to the pool. Also in this case the H_0 hypothesis could not be accepted.

Contrarily to the global comparison between the experiments conducted with the two model layouts, we highlight, only when Ω_M was applied, one noticeable difference. In fact, when inferring

on the true difference in means on a confidence level of 0.05, we could not reject the standard hypothesis H_0 . Hence, in this case, the data were not sufficiently reliable to detect a significant difference with respect to the deposited weights on the two different alluvial fans.

Conversely, the statistical analysis of the experiments conducted with Ω_F , all allowed corroborating the same set of hypotheses as in the case of the global comparison between alluvial fan model layouts.

2.2 Hazard – Exposure Analysis

In the supplementary material repository (Appendix 2 and 3, respectively) the reader has

direct access the whole set of results obtained by executing our experimental program, that is, for each model layout, 36 results in terms of $DA_s\%$ and $E_{w+s}\%$ associated to Ω_M and Ω_F , V_t , and $V_s\%$. Before explicitly unravelling how the exposure variables might be correlated to the hazard variables, we present in Table 5 the values of Pearson’s correlation coefficient for the set of relations, $w_f \sim DA_s\%$, $w_f \sim E_{w+s}\%$, and $DA_s\% \sim E_{w+s}\%$ in *UC* and *AC*. In Table 5 we first report the obtained correlation values for these relations discerning between model layouts but not between the adopted stream power regimes. Then, we report the correlation values for the same set of relations distinguishing also between adopted stream power regimes.

Table 4 Results of the normality checks for the weight datasets related to the experiments conducted with medium stream power, Ω_F , graphically summarized in the last 6 boxplots (from left to right) in Figure 5 by applying the Shapiro-Wilk test and specific comparison of the experimental results obtained for the two model layouts (unchanneled (*UC*) and artificially channeled (*AC*), respectively) by comparing the mean weights (kg) of the sediment remaining in the feeding channel, deposited on the alluvial fan and exported to the pool. *C*: feeding channel; *F*: alluvial fan surface; *P*: containment pool.

Part of the system (<i>C, F, P</i>)	<i>C</i>	<i>C</i>	<i>F</i>	<i>F</i>	<i>P</i>	<i>P</i>
Alluvial fan layout (<i>UC, AC</i>)	<i>UC</i>	<i>AC</i>	<i>UC</i>	<i>AC</i>	<i>UC</i>	<i>AC</i>
Stream power regime	Ω_F	Ω_F	Ω_F	Ω_F	Ω_F	Ω_F
Weight measures (<i>r</i> = remaining in the feeding channel; <i>d</i> = deposited on the alluvial fan; <i>e</i> = exported to the pool)	<i>r</i>	<i>r</i>	<i>d</i>	<i>d</i>	<i>e</i>	<i>e</i>
Shapiro-Wilk normality test W-value	0.89758	0.8745	0.94827	0.81511	0.88961	0.995655
Shapiro-Wilk normality test p-value	0.05216	0.02112	0.3986	0.002503	0.038	0.5366
Inference on normality on a 0.05 confidence level: (H_0 : data is normally distributed; H_1 : data is no normally distributed)	H_0 accepted	H_0 rejected	H_0 accepted	H_0 rejected	H_0 rejected	H_0 accepted
Welch Two Sample t-test applied	No		No		No	
Wilcoxon rank sum test	Yes		Yes		Yes	
Test parameter value (and degrees of freedom)	$W = 170$		$W = 258$		$W = 0$	
p-value	0.814		0.002514		3.222e-07	
Inference on true difference in means on a 0.05 confidence level: (H_0 : true difference in means is equal to 0; H_1 : true difference in means is not equal to 0)	H_0 accepted		H_0 rejected → the two populations are not identical		H_0 rejected → the two populations are not identical	

Table 5 Pearson’s correlation coefficient values for the following relations: deposited sediment on the fan vs. exposed area due to sediment deposition ($w_f \sim DA_s\%$), deposited sediment on the fan vs. exposed area due to sediment deposition and water flow ($w_f \sim E_{w+s}\%$), exposed area due to sediment deposition vs. exposed area due to sediment deposition and water flow ($DA_s\% \sim E_{w+s}\%$), considering the adopted model layout (unchanneled (*UC*) and artificially channeled (*AC*), respectively) and the imposed stream power regime (medium - Ω_M - and full - Ω_F -). Exposed areas are considered in % of the total alluvial fan area.

Experimental setting: alluvial fan layout, stream power regime	Correlation: $w_f \sim DA_s\%$	Correlation: $w_f \sim E_{w+s}\%$	Correlation: $DA_s\% \sim E_{w+s}\%$
<i>UC, \Omega_M + \Omega_F</i>	0.995	0.726	0.768
<i>AC, \Omega_M + \Omega_F</i>	0.955	0.912	0.928
<i>UC, \Omega_M</i>	0.952	0.813	0.923
<i>UC, \Omega_F</i>	0.957	0.773	0.693
<i>AC, \Omega_M</i>	0.952	0.962	0.977
<i>AC, \Omega_F</i>	0.962	0.853	0.837

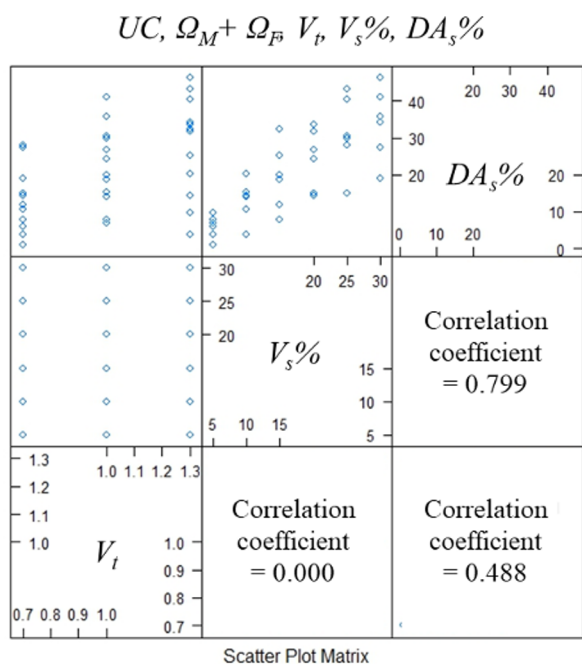


Figure 8 Scatter Plot Matrix involving the variables total volume - V_t , sediment fraction - $V_s\%$, and exposed area due to sediment deposition - $DA_s\%$ (arranged along the off diagonal) for the experimental setting (unchannelised alluvial fan (UC) irrespectively of the applied stream power ($\Omega_M + \Omega_F$). The upper triangular matrix (with respect to the off diagonal) contains the scatterplots of the row versus the column variable in the off diagonal. The cells of the lower triangular matrix contain the values of the Pearson's correlation coefficient between the corresponding row and column variables arranged along the off diagonal. Whereas correlation between V_t and $DA_s\%$ is "moderate", correlation between $V_s\%$ and $DA_s\%$ is "strong".

As can be appreciated from **Table 5** the value of the Pearson's correlation coefficient between the weight of the deposited sediment and the alluvial fan area covered with sediment was remarkably high (close to unity), irrespectively of the considered model layout and the imposed stream power. Correlation decreased between w_f and $E_{w+s}\%$ as well as between $DA_s\%$ and $E_{w+s}\%$. This decrease appeared more pronounced in case of the UC layout and with Ω_F . Considering, finally, the correlation between $DA_s\%$ between $E_{w+s}\%$ a similar patterns could be observed.

Hazard ($V_t, V_s\%$) end exposure variables ($DA_s\%$ and $E_{w+s}\%$) were correlated among each other in the defined six settings (i.e. [$UC, \Omega_M + \Omega_F$], [$AC, \Omega_M + \Omega_F$], [UC, Ω_M], [UC, Ω_F], [AC, Ω_M], [AC, Ω_F]). The resulting correlation values among hazard and exposure variables for the experimental

setting [$UC, \Omega_M + \Omega_F$] are shown exemplarily as scatterplot in **Figure 8**. In **Tables 6** and **7** we report the correlation matrices of the remaining experimental configurations between hazard variables and one of the two exposure variables ($DA_s\%$ or $E_{w+s}\%$), respectively. Obviously, the hazard variables were completely uncorrelated in all settings.

Table 6 Correlation matrices containing the values of the Pearson's correlation coefficients between hazard variables (total volume - V_t - and sediment fraction - $V_s\%$ -) and the exposed area measured in % of the alluvial fan area due to sediments, $DA_s\%$. "vw", "w", "m", "s", and "vs" mean "very weak", "weak", "moderate", "strong", and "very strong" correlation, respectively. Considered alluvial fan layouts: "unchannelised" and "artificially channeled alluvial fan (UC and AC , respectively); considered stream power regime: experiments without discerning between "medium" and "full" stream power, $\Omega_M + \Omega_F$; experiments applying "medium" stream power regime, Ω_M ; experiments applying "full" stream power regime, Ω_F .

Experimental configuration: UC, Ω_F			
	V_t	$V_s\%$	$DA_s\%$
V_t	1.000	0.000	0.439 → "m"
$V_s\%$	0.000	1.000	0.871 → "vs"
$DA_s\%$	0.439 → "m"	0.871 → "vs"	1.000
Experimental configuration: $AC, \Omega_M + \Omega_F$			
	V_t	$V_s\%$	$DA_s\%$
V_t	1.000	0.000	0.276 → "w"
$V_s\%$	0.000	1.000	0.792 → "s"
$DA_s\%$	0.276 → "w"	0.792 → "s"	1.000
Experimental configuration: AC, Ω_M			
	V_t	$V_s\%$	$DA_s\%$
V_t	1.000	0.000	0.351 → "w"
$V_s\%$	0.000	1.000	0.808 → "vs"
$DA_s\%$	0.351 → "w"	0.808 → "vs"	1.000
Experimental configuration: AC, Ω_F			
	V_t	$V_s\%$	$DA_s\%$
V_t	1.000	0.000	0.193 → "vw"
$V_s\%$	0.000	1.000	0.902 → "vs"
$DA_s\%$	0.193 → "vw"	0.902 → "vs"	1.000

Correlations between V_t and $V_s\%$ on the one hand and $DA_s\%$ and $E_{w+s}\%$ on the other hand were all positive as expected. We found that in general the correlation between $V_s\%$ and the exposure variable was stronger than the correlation between V_t and the exposure variable. Two noticeable exceptions were $\{UC, \Omega_M + \Omega_F, V_t, V_s\%, E_{w+s}\%$ and $\{UC, \Omega_F, V_t, V_s\%, E_{w+s}\%$. In the former case V_t and $E_{w+s}\%$ were moderately correlated and the correlation between $V_s\%$ and $E_{w+s}\%$ was weak, whereas in the latter case V_t and $E_{w+s}\%$ were

strongly correlated while the correlation between $V_s\%$ and $E_{w+s}\%$ was weak again. The correlation between $V_s\%$ (V_t) and $DA_s\%$ was systematically higher (lower) than when $E_{w+s}\%$ was taken as exposure variable. The experimental configurations that exhibited an at least “moderate” correlation between the two covariates (V_t and $V_s\%$) and the respective exposure variable were: 1) $\{UC, \Omega_M + \Omega_F, V_t, V_s\%, DA_s\%\}$ (“m” and “s”, respectively); 2) $\{UC, \Omega_F, V_t, V_s\%, DA_s\%\}$ (“m” and “vs”, respectively).

Table 7 Correlation matrices containing the values of the Pearson’s correlation coefficients between hazard variables (total volume - V_t - and sediment fraction - $V_s\%$ -) and the exposed area measured in % of the alluvial fan area due to both water and sediments, $E_{w+s}\%$.

Experimental configuration: $UC, \Omega_M + \Omega_F$			
	V_t	$V_s\%$	$E_{w+s}\%$
V_t	1.000	0.000	0.480 → “m”
$V_s\%$	0.000	1.000	0.400 → “w”
$E_{w+s}\%$	0.480 → “m”	0.400 → “w”	1.000
Experimental configuration: UC, Ω_F			
	V_t	$V_s\%$	$E_{w+s}\%$
V_t	1.000	0.000	0.682 → “s”
$V_s\%$	0.000	1.000	0.331 → “w”
$E_{w+s}\%$	0.682 → “s”	0.331 → “w”	1.000
Experimental configuration: $AC, \Omega_M + \Omega_F$			
	V_t	$V_s\%$	$E_{w+s}\%$
V_t	1.000	0.000	0.368 → “w”
$V_s\%$	0.000	1.000	0.690 → “s”
$E_{w+s}\%$	0.368 → “w”	0.690 → “s”	1.000
Experimental configuration: AC, Ω_M			
	V_t	$V_s\%$	$E_{w+s}\%$
V_t	1.000	0.000	0.388 → “w”
$V_s\%$	0.000	1.000	0.803 → “vs”
$E_{w+s}\%$	0.388 → “w”	0.803 → “vs”	1.000
Experimental configuration: AC, Ω_F			
	V_t	$V_s\%$	$E_{w+s}\%$
V_t	1.000	0.000	0.364 → “w”
$V_s\%$	0.000	1.000	0.559 → “m”
$E_{w+s}\%$	0.362 → “w”	0.559 → “m”	1.000

In [Appendixes 4, 5, 6, 7, 8, and 9](#) available as supplementary material we report the results of multiple linear regression analysis applied to investigate the combined effects of V_t and $V_s\%$ on $DA_s\%$. Hence, the linear model $DA_s\% = a_0 + a_1V_t + a_2V_s\% + \varepsilon$, where $DA_s\%$ is the response variable, V_t and $V_s\%$ are the explanatory variables, a_0, a_1 , and a_2 are the coefficients and ε is the

stochastic component, was fit to the data considering all experimental configurations.

In [Appendix 10, 11, 12, 13, 14, and 15](#) (available as supplementary material) we report the results of multiple linear regression analysis applied to investigate the combined effects of V_t and $V_s\%$ on $E_{w+s}\%$. Hence, the linear model $E_{w+s}\% = a_0 + a_1V_t + a_2V_s\% + \varepsilon$, where $E_{w+s}\%$ is the response variable, V_t and $V_s\%$ are the explanatory variables, a_0, a_1 , and a_2 are the coefficients and ε is the stochastic component, was fit to the data considering all experimental configurations.

In [Figure 9](#), the response and covariate data are plotted as dots in 3D space. The tilted planes represent the estimated models which describe how $DA_s\%$ and $E_{w+s}\%$ are expected to change in response to V_t and $V_s\%$, respectively. Physically unfeasible responses (i.e. $DA_s\% < 0\%$ and $E_{w+s}\% < 0\%$) are detectable in the graphs by the vanishing multiple linear regression planes (i.e. sectors where the planes would protrude into the negative response regions).

From a statistical standpoint the obtained multiple linear regression models with $DA_s\%$ as response variable are all characterized by an overall satisfactory goodness of fit (i.e., Multiple and Adjusted $R^2 > 0.7$). In addition, the F-statistic and the associated p-values indicate that globally there is a solid relationship between the set of explanatory variables and the considered response variable. The medians of the distributions of the residuals are sufficiently close to zero and these distributions are approximately symmetrical. The effects of the individual explanatory variables on the expected value of the response variable are, generally, at least significant ($\Pr(>|t|) < 0.05$). One notable exception was encountered in one of the model coefficients in the following experimental configuration: $\{AC, \Omega_F\}$: (a_1). As expected the exposure due to sediment deposition only, $DA_s\%$, was higher on the UC alluvial fan irrespectively of the imposed stream power (i.e. larger intercept values a_0 and overall comparable coefficient values, a_1 and a_2 respectively).

When discerning between stream power regimes with the UC alluvial fan layout expected the values of the response variable, $DA_s\%$, were higher when Ω_F was imposed.

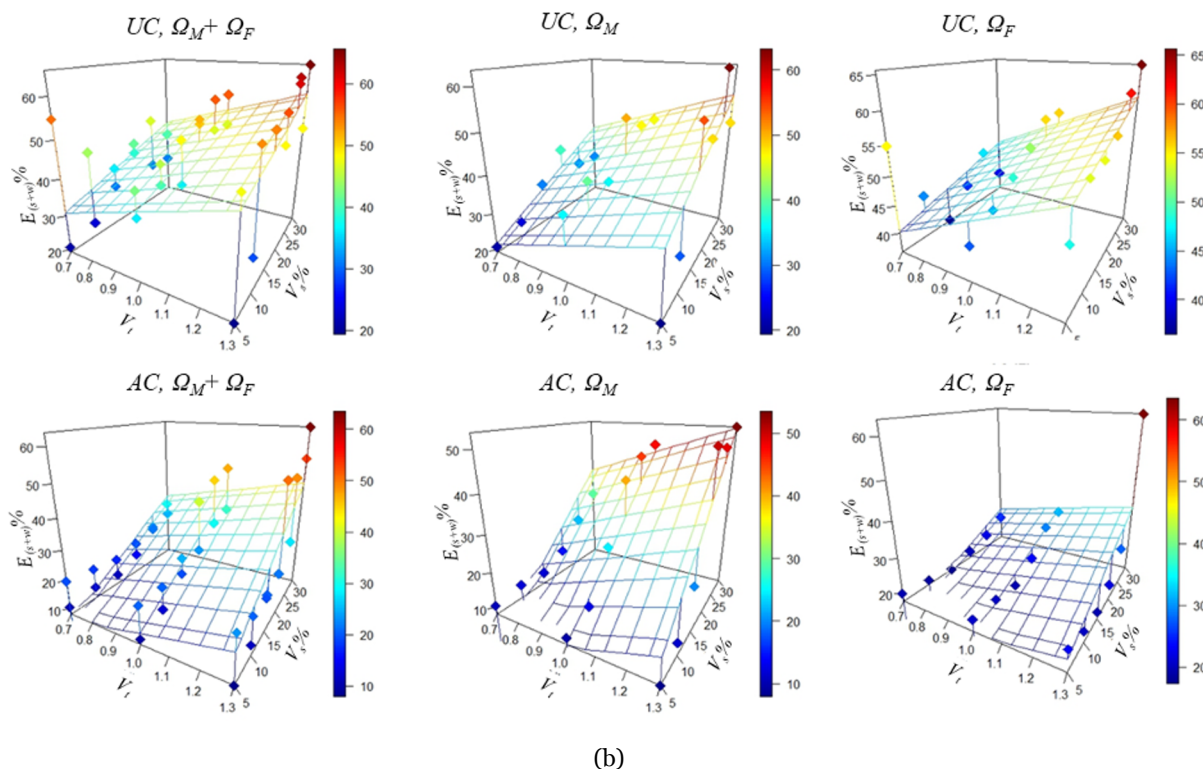
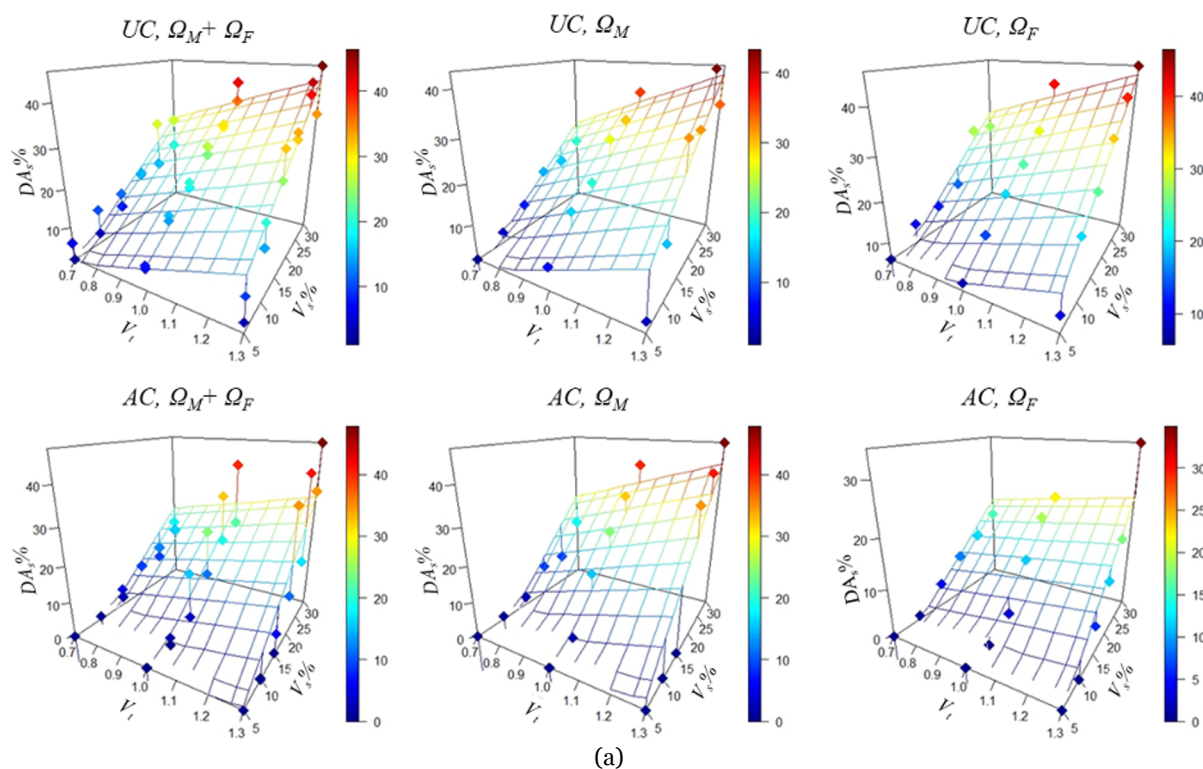


Figure 9 Multiple linear regression planes (i.e. visualized expected values of the response variables exposed area of the alluvial fan due to sediment deposition ($DA_s\%$) (a) and sediment deposition and water flow conjointly ($E_{w+s}\%$) (b), depending on the values of the explanatory variables, total volume - V_t - and sediment fraction - V_s %- and values of the response variable represented as dots associated to the experimentally chosen values of the explanatory variables for the “unchannelised” and “artificially channeled” alluvial fan layout (unchanneled (UC) and artificially channeled (AC), respectively) and applying the “medium” and “full” stream power regimes (Ω_M and Ω_F , respectively).

When considering the *AC* alluvial fan layout, the opposite was the case. When $E_{w+s}\%$ was considered as response variable and, hence, the multiple linear model, $E_{w+s}\% = a_0 + a_1V_t + a_2V_s\% + \varepsilon$ was fit to the data, in almost all experimental configurations, a smaller percentage of the variance found in the response variable could be explained by the explanatory variables. The Multiple and Adjusted R^2 values were significantly smaller than 0.7 with one exception (i.e. configuration: $\{AC, \Omega_M\}$). In four out of six considered multiple linear regression models at least one of the three model coefficients did not exhibit a significant effect on the response variable as indicated by the t-statistics and the associated Pr ($>|t|$) values. The less satisfactory performance of this second set of multiple linear regression models indicate that V_t and $V_s\%$ alone, are not sufficient as predictors. Cautiously interpreting the obtained results when $E_{w+s}\%$ was considered as response variable the general trends described above for the multiple linear regression models with $DA_s\%$ as response variable seem to be mirrored, although in the *UC* layout case the $DA_s\%$ values were comparable with both applied stream power regimes.

3 Discussion

The dynamics occurring on the two alluvial fan types were different due to their morphological and topographic features. The main factor influencing the processes was the presence or absence of the artificial channel, which confined the flow reducing the flooded zones.

Maintaining all the loading conditions equal, the artificially channeled alluvial fan (*AC*) surface was almost always less exposed than the unchanneled alluvial fan system (*UC*). Expectedly the amount of sediment reaching the pool in the *AC* system was higher according to the associated sediment budgets.

Moreover, the experimental runs on the artificially channeled fan showed more homogeneous exposure patterns with respect to the *UC* system runs, since the guiding channel limited the flow to freely migrate on the alluvial fan surface.

Runs conducted in the *UC* setting showed that total event volume had a great influence on exposure when imposing Ω_F . A few exceptions,

however, were not in line with what seemed to be a credible trend. Combining a 5% volumetric sediment percentage experiment with Ω_F showed, for instance, highest exposure for the 0.7 L total volume, in clear contradiction to the previously described main trend.

The other cases whose results diverged from the positive relationship between exposure and total volume were those experimental runs where Ω_M was applied and volumetric sediment percentages of 5, 10, and 20% were imposed. In those cases, highest exposures were retraced when the medium total volume (1.0 L) was employed. The appearance of prolonged self-channelization phenomena observed with an employed total volume of 1.3 L could be one plausible explanation of these observations.

In *AC* the experimental runs conducted by applying a Ω_M showed a positive relationship between total event volume and exposure (for sediment volumetric sediment percentages equal or higher than 20%). When Ω_F was imposed this positive relationship became more pronounced, even if, when increasing the volumetric sediment percentage from 20% to 25% the change from 1.0 L to 1.3 L resulted in a slight reduction of the exposed area.

On the *UC*, exposure was generally higher for the Ω_F regime with respect to Ω_M . This pattern could be consistently retraced for the total volumes of 0.7 and 1.0 L and for all volumetric sediment percentage.

Two cases showed higher exposure values for the Ω_M scenario: the experiments with a volumetric sediment percentage of 15 and 25%, both involving the highest total event volume. The 15% run behavior can be explained observing in detail the morphodynamics of the distributary process by careful video inspection. Imposing medium stream power with this specific volumetric sediment percentage a peculiar flow behavior could be observed. In the upper part of the alluvial fan, a small deposition formed and, after an initial blockage, determined a flow diversion into two main paths. The same volumetric sediment percentage combined with Ω_F did not cause the initial deposition phase and resulted in a lower exposure because the highest transport capacity of water avoided further small depositions.

The experiments conducted in *AC* presented a

partially negative exposure-stream power response, appreciable incrementing the volumetric sediment percentage from 15% to 25%. We think that this behavior can be linked to alluvial fan structure itself. While when imposing Ω_M bridge occlusion, a back-filling deposition in the channel and fan flooding started to appear with a volumetric sediment percentage of 20%, Ω_F allowed the sediment to flow efficiently below the bridge. In fact, with this flow regime, most of the sediments were transported to the lowest part of the fan. There deposition could start due to the abrupt change of slope between fan and pool. This downstream accumulation is impeded in real confluences as long as the receiving river has a sufficient transport capacity to entrain and transport the newly fed sediment. Contrarily, at confluences between torrents and rivers not competent enough to mobilize considerable amounts of the fed sediment, backfilling processes can be generated and head-ward propagating hazards may result (see Harvey 2012, for a review).

The volumetric sediment percentage, understood as availability of sediment set as initial loading condition in the feeding channel, appeared to be the variable with the most complex influence on exposure.

Concerning the experiments conducted in the unchanneled alluvial fan model, the volumetric sediment percentage alone seems not to be a good proxy for exposure. In fact, in the medium stream power scenario the resulting relationship was not linear and the maximum exposure did not correspond to the highest volumetric sediment percentage (30%). It is possible to assume that for Ω_M events, as it was the case for the experiments conducted with 0.7 and 1.0 L, there is a specific sediment volumetric sediment percentage that can be associated with the maximum exposure, if all the other loading conditions are maintained constant. In fact, when this specific volumetric sediment percentage was exceeded, a decreasing exposure trend resulted due to less frequent avulsion phenomena caused by a higher deposition on the fan that partially impeded further lateral shifts.

A full stream power regime, together with an increasing volumetric sediment percentage, generated a quite constantly growing exposure, except when applying the smallest total event

volume (0.7 L). In that specific case the stream power-exposure relationship was negative for the lowest and highest sediment fractions, respectively.

Sediment fraction on the AC fan showed more defined exposure trends with respect to the UC ones.

To sum up, this study was necessary to deepen the knowledge on risk exposure generated by flood events occurring on alluvial fans. Event magnitude seemed an immediately available and appropriated concept to describe event processes characteristics but through an extended literature review we realized that it has sometimes been described with the general term of “event size” or “flood size” (Simpson et al. 2013; Hooke 2016) and defined by a plethora of mostly isolated variables such as peak discharge (Gray et al. 2018), combination of water discharge and recurrence interval (Salgueiro et al. 2013), stream power (Magilligan 1992; Cenderelli and Wohl 2003), flood duration (Dean and Schmidt 2013), sediment mobility and bedload (Rainato et al. 2017), resulting in a multitude of proxies and hence in detrimental vagueness. Therefore, due to this lack in an unambiguous definition of magnitude, this study aimed at exploring how different loading conditions and specific alluvial fan designs together, exert a tangible influence on exposure as a result of the morphodynamic processes taking place on the unconfined and convex shaped alluvial fan surfaces.

We contend that precisely this synoptic appraisal be beneficial for flood hazard and risk management on alluvial fans. The study was performed by means of an experimental alluvial fan model featuring two different fan surfaces respectively representing a pristine alluvial fan (UC) and an alluvial fan modified by human intervention (AC), where a series of laboratory experiments were run to investigate the topic in detail by following a ‘similarity of process concept’ (Hooke 1968). Despite the approach is not exempt from some limitations, it was possible to discard the scale issue due to the theoretical nature of the study, which did not require the perfect representation of a real-world prototype.

Although the ideal experimental setting would feature an erodible surface to monitor incision below the original fan surface, the non-erodible fan surface adopted allowed anyway to gain insights about the distributary processes, and partially

captured channelisation and self-confining flows on previously deposited material.

As expected, the interactions among the tested loading configuration variables were very complex as they produced different exposures according to the initial variable values combinations. All the tested loading variables had remarkable effects on exposure and the experimental results seemed to suggest, but not conclusively, that exposure might be positively related to several of them.

In fact, more than one experiment highlighted a negative relationship, showing that a higher exposure, contrarily to what is suggested by common thought, does not always correspond to higher values of the loading parameters. This led to the insight that event magnitude alone, even if rigorously defined in terms of a consistent set of characterizing parameters, is a poor proxy for exposure. Our results rather indicate that exposure might depend on the coupled effects of several variables and our future research program will be devoted to unveil these coupled effects and to establish quantitative relationships.

The performed experiments showed that autogenic distributary processes may play a crucial role in determining exposure of alluvial fans as already reported by Whipple et al. (1998), Muto et al. (2007), and van Dijk et al. (2008, 2009). In this context, it is intrinsically difficult to predict time and location of sudden avulsion and channelisation processes, which may significantly alter the resulting patterns of exposure. With respect to the employed alluvial fan type, it was possible to detect that in *UC* avulsions and subsequent channelisation emerge as pivotal phenomena, whereas in *AC* back-stepping deposition in the guiding channel followed by subsequent outburst turned out to be crucial.

In Figure 10 the distributary effect due to these processes is exemplarily shown. Quantifying the effects of exposure due to the aforementioned suit of processes requires further research efforts and is a high priority in our future research agenda.

The experimental program foresaw only one experiment for each combination of values with respect to all loading variables.

In this regard, we prospect to extend systematically the experimental program as to assess the randomness associated to exposure resulting from a specified loading configuration. As

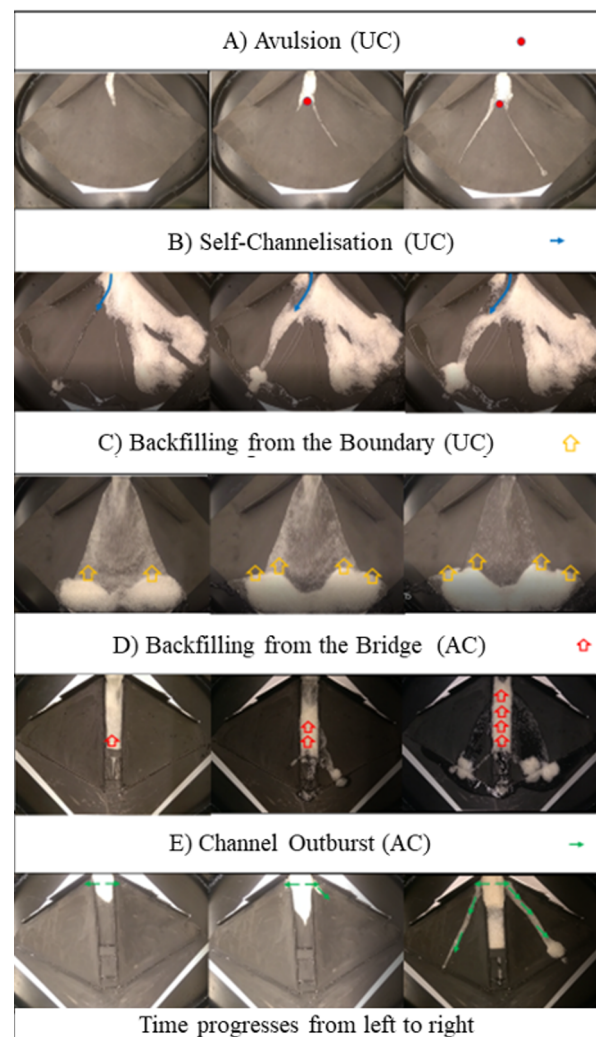


Figure 10 Geomorphic processes at work directly influencing the distributary dynamics and, hence, exposure: A) avulsion; B) self-channelisation; C) backfilling from the boundary. D) backfilling from the bridge and E) channel outburst. Notice that A, B and C occurred on the “unchannelised” alluvial fan (*UC*), whereas D and E occur on the “artificially channelled” alluvial fan (*AC*).

to explore the potential relevance of this topic we repeated the experiment for one specific loading configuration (i.e. topographic setting: *UC*; $V_t = 1$ L; $V_s\% = 15\%$; stream power regime: Ω_M) eight times. The deposited mass on the alluvial fan surface ranged from a minimum of 0.21 kg to a maximum of 0.264 kg with an average weight value of 0.239 kg and a standard deviation of 0.018 kg. As expected also absolute exposure varied from 22.0% to 38.9% of the alluvial fan surface area (mean = 34.0%; standard deviation = 5.4%).

4 Conclusions

Alluvial fans have become preferential areas to settle human activities in mountain regions all around the world (Antronico et al. 2014). The occurrence of extreme flood events impels risk managers to determine hazard exposure. As attested by the specific literature, experimental models are useful research instruments to study alluvial fan processes and to specifically assess the role of autogenic behavior and its effect on exposure (Schumm et al. 1987; Zarn and Davies 1994; Bryant et al. 1995; Cole 2001; Davies et al. 2003; Muto et al. 2007; Van Dijk et al. 2012; Guerit et al. 2014; Clarke 2015; Sturm et al. 2018a and 2018b). In this study a series of 72 laboratory experiments has been carried out following the basic principle of the ‘similarity of process concept’, which justified the theoretical study of fan processes and avoiding scale issues related to models reproducing real prototypes. The attention was oriented to identify relationships among the risk equation variables, in particular between magnitude and exposure. Due to the vagueness of magnitude concept, the concept of system loading configuration was preferred to ensure a comprehensive assessment of the conditions the experimental model runs were subjected to. Therefore, the aim of the work was to explore how different loading conditions and specific alluvial fan designs exert a tangible influence on exposure because of the morphodynamic processes taking place on the unconfined and convex shaped alluvial fan surfaces. The considered loading conditions were stream power, total event volume and volumetric sediment percentage and they were tested on two different fan surfaces, an unchanneled alluvial fan and an artificially channeled alluvial fan, both non-erodible systems.

Analyzing and resuming the results, the research highlighted the main differences on dynamics occurring on an ‘unchanneled’ alluvial fan (*UC*) and modified alluvial fan by human intervention (*AC*). The first is characterized by a morphological shape that favors the free flow migration which is instead limited in the second fan type since the presence of a guiding channel constituted a strong impediment for avulsion processes. For this reason, the exposure resulting from experiments run on the *UC* involved

consistent portions of the fan surface, generally more extended than the exposed areas that have been detected in the *AC* system.

Moreover, as expected, the results underlined a complex interaction among the system loading parameters and other system processes such as deposition, avulsion and channelization that, operating together, concur to determine the overall exposure. All the variables employed for the experiments showed scenarios having positive relation with exposure, but more than one experiment proved that a higher exposure not always corresponded to higher values of loading parameters.

Autogenic behavior may be responsible for the observed deviations from expected trends (i.e. higher exposure related to higher values of the loading parameters).

We remark that still knowledge gaps need to be filled to comprehensively understand how the geomorphic processes interact and ultimately determine hazard exposure; and that potential biases related to the roughness characteristics of the employed surface materials have to be carefully considered.

We argue that the field of experimental alluvial fan models represents a promising research topic. For instance, the experimental program presented in this study could be extended by considering a convenient number of repetitions of each experimental configuration as to specifically assess the randomness of distributary processes. Moreover, erodible alluvial fan models could be employed to analyze erosion and deposition dynamics by means of Geomorphic Change Detection specific software or using DEM differencing (James et al. 2012). This task would require elevation data, which could be obtained by a “structure from motion” technique (Westoby et al. 2012). Using this technique, three dimensional images could be obtained starting from at least three two-dimensional ones. The use of fixed high-resolution simultaneous-shoot cameras would enhance data acquisition.

Based on the insights of our experimental study hazard and risk managers are forewarned that a computational simulation of biphasic processes alone, of course specified both in terms of their loading parameters and their recurrence interval, may still be insufficient for a rigorous

spatial delimitation of exposure on alluvial fans. The complexity of distributary dynamics observed in our experiments is, in fact, remarkable and predicting both spatially and temporally autogenic behavior constitutes a major challenge (De Haas et al. 2018). Hence, we argue that the experimental approach should be seriously considered as a complement to the traditionally employed methods

Acknowledgements

The authorship acknowledges the support of the following 2 research projects: Project FONDECYT nr. 1170657 titled “The flood memory of a river system: using both experimental and field-based approaches to unravel the role of unsteady flow and antecedent flows on sediment dynamics during floods” funded by CONICYT and led by Luca Mao; Project FONDECYT nr. 1170413 titled “Morphological impacts in rivers affected by

in hazard and risk assessment. Laboratory experimental models proved useful in highlighting the subtleties of distributary dynamics and how variable the effects on exposure can be.

Finally, these models can be employed as a testbed for improved 2D biphasic hydrodynamic simulation models for a reliable hazard assessment on settled alluvial fans.

volcanic eruptions. Chaiten and Calbuco: similar disturbance but different fluvial evolution? (PIROFLUV)” funded by CONICYT and led by Andrés Iroumé.

Electronic supplementary material: Supplementary materials (Appendixes 1-15) are available in the online version of this article at <https://doi.org/10.1007/s11629-018-5788-x>

References

- Anstey RL (1965) Physical characteristics of alluvial fans. Natick, MA: Army Natick Laboratory, Technical Report, ES-20.
- Antronico L, Greco R, Robustelli G, et al. (2015) Short-term evolution of an active basin-fan system, Aspromonte, south Italy. *Geomorphology* 228: 536-551. <https://doi.org/10.1016/j.geomorph.2014.10.013>
- Blair TC, McPherson JG (1994) Alluvial fans and their natural distinction from rivers based on morphology, hydraulic processes, sedimentary processes, and faces assemblages. *Journal of Sedimentary Research* 64: 451-490. <https://doi.org/10.1306/D4267DDE-2B26-11D7-8648000102C1865D>
- Blair TC, McPherson JG (2009) Processes and forms of alluvial fans. *Geomorphology of desert environments*. Springer, Dordrecht: 413-467. https://doi.org/10.1007/978-1-4020-5719-9_14
- Bryant M, Falk P, Paola C (1995) Experimental study of avulsion frequency and rate of deposition. *Geology* 23 (4): 365-368. [https://doi.org/10.1130/0091-7613\(1995\)023<0365:ESOFAFA>2.3.CO;2](https://doi.org/10.1130/0091-7613(1995)023<0365:ESOFAFA>2.3.CO;2)
- Bull WB (1977) The alluvial-fan environment. *Progress in Physical Geography* 1(2): 222-270. <https://doi.org/10.1177/030913337700100202>
- Cenderelli DA, Wohl EE (2003) Flow hydraulics and geomorphic effects of glacial - lake outburst floods in the Mount Everest region, Nepal. *Earth Surface Processes and Landforms* 28 (4): 385-407. <https://doi.org/10.1002/esp.448>
- Clarke LE (2015) Experimental alluvial fans: Advances in understanding of fan dynamics and processes. *Geomorphology* 244: 135-145. <https://doi.org/10.1016/j.geomorph.2015.04.013>
- Clarke L, Quine TA, Nicholas A (2010) An experimental investigation of autogenic behavior during alluvial fan evolution. *Geomorphology* 115 (3-4): 278-285. <https://doi.org/10.1016/j.geomorph.2009.06.033>
- Clevis Q, de Boer P, Wachter M (2003) Numerical modelling of drainage basin evolution and three-dimensional alluvial fan stratigraphy. *Sedimentary Geology* 163 (1-2): 85-110. [https://doi.org/10.1016/S0037-0738\(03\)00174-X](https://doi.org/10.1016/S0037-0738(03)00174-X)
- D'Agostino V, Cesca M, Marchi L (2009) Field and laboratory investigations of runout distances of debris flows in the Dolomites (Eastern Italian Alps). *Geomorphology* 115 (3-4): 294-304. <https://doi.org/10.1016/j.geomorph.2009.06.032>
- Davies TRH, McSaveney MJ, Clarkson PJ (2003) Anthropogenic aggradation of the Waiho River, Westland, New Zealand: microscale modelling. *Earth Surface Processes and Landforms* 28: 209-218. <https://doi.org/10.1002/esp.449>
- De Haas T, Densmore AL, Stoffel M, et al. (2018) Avulsions and the spatio-temporal evolution of debris-flow fans. *Earth-Science Reviews* 177: 53-75. <https://doi.org/10.1016/j.earscirev.2017.11.007>
- Dean DJ, Schmidt JC (2013) The geomorphic effectiveness of a large flood on the Rio Grande in the Big Bend region: Insights on geomorphic controls and post-flood geomorphic response. *Geomorphology* 201: 183-198. <https://doi.org/10.1016/j.geomorph.2013.06.020>
- Drew F (1873) Alluvial and lacustrine deposits and glacial records of the Upper-Indus Basin. *Quarterly Journal of the Geological Society* 29(1-2): 441-471. <https://doi.org/10.1144/GSL.JGS.1873.029.01-02.39>
- Fuchs S (2009) Susceptibility versus resilience to mountain hazards in Austria-paradigms of vulnerability revisited. *Natural Hazards and Earth System Sciences* 9: 337-352. <https://doi.org/10.5194/nhess-9-337-2009>
- Fuchs S, Keiler M, Zischg A (2015) A spatiotemporal multi-hazard exposure assessment based on property data. *Natural Hazards and Earth System Sciences* 15(9): 2127-2142. <https://doi.org/10.5194/nhess-15-2127-2015>
- Fuchs S, Karagiorgos K, Kitikidou K, et al. (2017a) Flood risk perception and adaptation capacity: a contribution to the socio-hydrology debate. *Hydrology and Earth System Sciences* 21(6): 3183-3198.

- <https://doi.org/10.5194/hess-21-3183-2017>
Fuchs S, Röthlisberger V, Thaler T, et al. (2017b) Natural hazard management from a co-evolutionary perspective: exposure and policy response in the European Alps. *Annals of the American Association of Geographers* 107(2): 382-392. <https://doi.org/10.1080/24694452.2016.1235494>
- Gray AB, Pasternack GB, Watson EB (2018) Estuarine abandoned channel sedimentation rates record peak fluvial discharge magnitudes. *Estuarine, Coastal and Shelf Science* 203: 90-99. <https://doi.org/10.1016/j.ecss.2018.02.007>
- Guerit L, Métivier F, Devauchelle O, et al. (2014) Laboratory alluvial fans in one dimension. *Physical Review* 90: 022203. DOI: 10.1103/PhysRevE.90.022203
- Harvey AM (2012) The coupling status of alluvial fans and debris cones: a review and synthesis. *Earth Surface Processes and Landforms* 37(1): 64-76. <https://doi.org/10.1002/esp.2213>
- Hooke RL (1968) Model geology: prototype and laboratory streams: discussion. *Geological Society of America Bulletin* 79: 391-394. [https://doi.org/10.1130/0016-7606\(1968\)79\[391:M GPALS\]2.0.CO;2](https://doi.org/10.1130/0016-7606(1968)79[391:M GPALS]2.0.CO;2)
- James LA, Hodgson ME, Ghoshal S, et al. (2012) Geomorphic change detection using historic maps and DEM differencing: The temporal dimension of geospatial analysis. *Geomorphology* 137 (1): 181-198. <https://doi.org/10.1016/j.geomorph.2010.10.039>
- Kain CL, Rigby EH, Mazengarb C (2018) A combined morphometric, sedimentary, GIS and modelling analysis of flooding and debris flow hazard on a composite alluvial fan, Caveside, Tasmania. *Sedimentary Geology* 364: 286-301. <https://doi.org/10.1016/j.sedgeo.2017.10.005>
- Magilligan FJ (1992) Thresholds and the spatial variability of flood power during extreme floods. *Geomorphology* 5:3-5: 373-390. [https://doi.org/10.1016/0169-555X\(92\)90014-F](https://doi.org/10.1016/0169-555X(92)90014-F)
- Mazzorana B, Fuchs S (2010) A conceptual planning tool for hazard and risk management. In: Chen SC (ed.), *Internationales Symposium Interpraevent in the Pacific Rim*, Klagenfurt: Internationale Forschungsgesellschaft Interpraevent: 828- 837.
- Mazzorana B, Nardini A, Comiti F, et al. (2017a) Toward participatory decision-making in river corridor management: two case studies from the European Alps. *Journal of Environmental Planning and Management* 61(7): 1250-1270. <https://doi.org/10.1080/09640568.2017.1339593>
- Mazzorana B, Iribarren P, Oyarzun C, et al. (2017b) Determining patterns of flood hazard exposure on an experimental alluvial fan. *Proceedings XX Congreso Geológico Argentino, Tucumán (7th-11th august)*, Technical session 3: 24-28.
- Mazzorana B, Ruiz-Villanueva V, Marchi L, et al. (2018) Assessing and mitigating large wood-related hazards in mountain streams: recent approaches. *Journal of Flood Risk Management* 11: 207-222. <https://doi.org/10.1111/jfr3.12316>
- Muto T, Steel RJ, Swenson JB (2007). Autostratigraphy: a framework norm for genetic stratigraphy. *Journal of Sedimentary Research* 77: 2-12. <https://doi.org/10.2110/jsr.2007.005>
- Paola C, Straub K, Mohrig D, et al. (2009) The “unreasonable effectiveness” of stratigraphic and geomorphic experiments. *Earth-Science Reviews* 97: 1-43. <https://doi.org/10.1016/j.earscirev.2009.05.003>
- Papathoma-Köhle M, Gerns B, Sturm M, et al. (2017) Matrices, curves and indicators: a review of approaches to assess physical vulnerability to debris flows. *Earth-Science Reviews* 171: 272-288. <https://doi.org/10.1016/j.earscirev.2017.06.007>
- Pelletier JD, Mayer L, Pearthree PA, et al. (2005) An integrated approach to flood hazard assessment on alluvial fans using numerical modeling, field mapping, and remote sensing. *Geological Society of America Bulletin* 117(9-10): 1167-1180. <https://doi.org/10.1130/B255440.1>
- Rainato R, Mao L, Picco L (2017) Near-bankfull floods in an Alpine stream: Effects on the sediment mobility and bedload magnitude. *International Journal of Sediment Research* 33(1): 27-34. <https://doi.org/10.1016/j.ijsrc.2017.03.006>
- Reitz MD, Jerolmack DJ (2012) Experimental alluvial fan evolution: Channel dynamics, slope controls, and shoreline growth. *JGR Earth Surface* 117: F02021. <https://doi.org/10.1029/2011JF002261>
- Röthlisberger V, Zischg AP, Keiler M (2017) Identifying spatial clusters of flood exposure to support decision making in risk management. *Science of the Total Environment* 598: 593-603. <https://doi.org/10.1016/j.scitotenv.2017.03.216>
- Salgueiro AR, Machado MJ, Barriendos M, et al. (2013) Flood magnitudes in the Tagus River (Iberian Peninsula) and its stochastic relationship with daily North Atlantic Oscillation since mid-19th Century. *Journal of Hydrology* 502: 191-201. <https://doi.org/10.1016/j.jhydrol.2013.08.008>
- Sanchez-Núñez JM, Macías JL, Saucedo R, et al. (2015) Geomorphology, internal structure and evolution of alluvial fans at Motozintla, Chiapas, Mexico. *Geomorphology* 230: 1-12. <https://doi.org/10.1016/j.geomorph.2014.10.003>
- Santangelo N, Santo A, Di Crescenzo G, et al. (2011) Flood susceptibility assessment in a highly urbanized alluvial fan: the case study of Sala Consilina (southern Italy). *Natural Hazards and Earth System Sciences* 11: 2765-2780. <https://doi.org/10.5194/nhess-11-2765-2011>
- Schumm SA, Mosley MP, Weaver WE (1987) *Experimental Fluvial Geomorphology*. Wiley Interscience, New York. p 413.
- Sturm M, Gerns B, Keller F, et al. (2018a) Experimental analyses of impact forces on buildings exposed to fluvial hazards. *Journal of Hydrology* 565: 1-13. <https://doi.org/10.1016/j.jhydrol.2018.07.070>
- Sturm M, Gerns B, Keller F, et al. (2018b) Understanding impact dynamics on buildings caused by fluvial sediment transport. *Geomorphology* 321: 45-59. <https://doi.org/10.1016/j.geomorph.2018.08.016>
- Van Dijk M, Kleinhans MG, Postma G, et al. (2012) Contrasting morphodynamics in alluvial fans and fan deltas: effect of the downstream boundary. *Sedimentology* 59 (7): 2125-2145. <https://doi.org/10.1111/j.1365-3091.2012.01337.x>
- Westoby MJ, Brasington J, Glasser NF, et al. (2012) Structure-from-Motion photogrammetry: A low-cost, effective tool for geoscience applications. *Geomorphology* 179: 300-314. <https://doi.org/10.1016/j.geomorph.2012.08.021>